

# **DELINEATION OF LANDSLIDE, FLASH FLOOD, AND DEBRIS FLOW HAZARDS IN UTAH**

Proceedings of a Specialty Conference  
Held At  
Utah State University, Logan, Utah  
June 14-15, 1984

Edited By  
David S. Bowles

GENERAL SERIES  
UWRL/G-85/03

Utah Water Research Laboratory  
Utah State University  
Logan, Utah 84322-8200

August 1985



# Dam Breach Erosion Modeling

A BREACH EROSION MODEL FOR EARTHEN DAMS

by D.L. Fread\*

ABSTRACT. A physically based mathematical model (BREACH) to predict the discharge hydrograph emanating from a breached earthen dam is presented. The earthen dam may be man-made or naturally formed by a landslide. The model is developed by coupling the conservation of mass of the reservoir inflow, spillway outflow, and breach outflow with the sediment transport capacity of the unsteady uniform flow along an erosion-formed breach channel. The bottom slope of the breach channel is assumed to be essentially that of the downstream face of the dam. The growth of the breach channel is dependent on the dam's material properties ( $D_{50}$  size, unit weight, friction angle, cohesive strength, and flow resistance factor), and an empirical factor which accounts for the effects of a grass cover. The model considers the possible existence of the following complexities: 1) core material having properties which differ from those of the downstream face of the dam; 2) the necessity of forming an eroded ditch along the downstream face of the dam prior to the actual breach formation by the overtopping water; 3) enlargement of the breach through the mechanism of one or more sudden structural collapses due to the hydrostatic pressure force exceeding the resisting shear and cohesive forces; 4) enlargement of the breach width by slope stability theory; and 5) initiation of the breach via piping with subsequent progression to a free surface breach flow. The outflow hydrograph is obtained through a time-stepping iterative solution that requires only a few seconds for computation on a main-frame computer. The model is not subject to numerical stability or convergence difficulties. The model's predictions are compared with observations of a piping failure in the man-made Teton Dam in Idaho and a breached landslide-formed dam in Peru. Also, the model has been used to predict possible downstream flooding from a potential breach of the landslide blockage of Spirit Lake in the aftermath of the eruption of Mount St. Helens in Washington. Model sensitivity to numerical parameters is minimal; however, it is sensitive to the material cohesion, friction angle, and the empirical grass cover factor when simulating man-made dams and to the cohesion and flow resistance factor when simulating landslide-formed dams.

\*D. L. Fread is a Senior Research Hydrologist with the Hydrologic Research Laboratory, National Weather Service, NOAA, Silver Spring, Maryland 20910.

## INTRODUCTION

Earthen dams are subject to possible failure from either overtopping or piping water which erode a trench (breach) through the dam. The breach formation is gradual with respect to time and its width as measured along the crest of the dam usually encompasses only a portion of the dam's crest length. In many instances, the bottom of the breach progressively erodes downward until it reaches the bottom of the dam; however, in some cases, it may cease its downward progression at some intermediate elevation between the top and bottom of the dam. The size of the breach, as constituted by its depth and its width (which may be a function of the depth), and the rate of the breach formation determine the magnitude and shape of the resulting breach outflow hydrograph which is of vital interest to hydrologists and engineers concerned with real-time forecasting or evacuation planning for floods produced by dam failures.

This paper presents a mathematical model (BREACH) for predicting the breach outflow hydrograph. The model is physically based on the principles of hydraulics, sediment transport, soil mechanics, the geometric and material properties of the dam, and the reservoir properties (storage volume, spillway characteristics, and time dependent reservoir inflow rate). The dam may be either man-made or naturally formed as a consequence of a landslide. In either, the mechanics of breach formation are very similar, the principal difference being one of scale. The landslide-formed dam is often much larger than even the largest of man-made earthen dams as illustrated in Fig. 1. The critical material properties of the dam are the internal friction angle, cohesion strength, and average grain size diameter ( $D_{50}$ ).

The breach erosion model presented herein for synthesizing a dam-breach outflow hydrograph differs from the parametric approach which the author has used in the NWS DAMBRK Model (Fread, 1977, 1981, 1983). The parametric model uses empirical observations of previous dam failures such as the breach width-depth relation, time of breach formation, and depth of breach to develop the outflow hydrograph. The breach erosion model presented herein can provide some advantages over the parametric breach model for application to man-made dams since the critical properties used by the model are measurable or can be estimated within a reasonable range from a qualitative description of the dam materials. However, it should be emphasized that even if the properties can be measured there is a range for their probable value and within this range outflow hydrographs of varying magnitude and shape will be produced by the model. The hydrologist or engineer should investigate the most critical combination of values for the dam's material properties. It is considered essential when predicting breach outflows of landslide dams to utilize a physically based model since observations of such are essentially non-existent, rendering the parametric approach infeasible.

In this paper, the breach erosion model is applied to the piping failure of the man-made Teton Dam in Idaho, the overtopping failure of the Mantaro landslide-formed dam in Peru, and the possible failure of the recently formed landslide blockage of Spirit Lake, near Mount St. Helens in Washington.

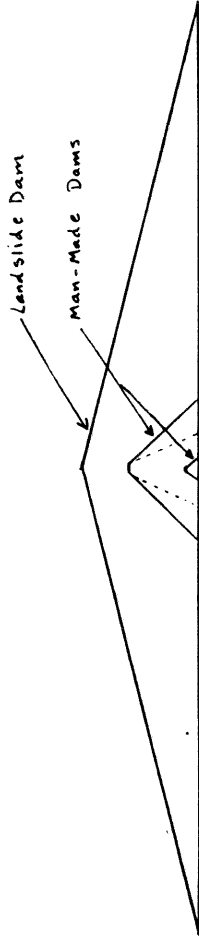


Figure 1 - Comparative View of Natural Landslide Dams and Man-Made Dams.

## PREVIOUS RESEARCH

Other investigators of dam breach outflows have developed physically based models.

The first was Cristofano (1967) who derived an equation which related the force of the flowing water through the breach to the shear strength of the soil particles on the bottom of the breach and in this manner developed the rate of erosion of the breach channel as a function of the rate of change of water flowing through the breach. He assumed the breach bottom width to be constant with time and always of trapezoidal shape in which the side slopes of the trapezoid were determined by the angle of repose of the breach material, and the bottom slope of the breach channel was equal to the internal friction angle of the breach material. An arbitrary empirical coefficient which was critical to the model's prediction was also utilized.

Harris and Wagner (1967) used the Schoklitsch sediment transport equation and considered the breach to commence its downward progression immediately upon overtopping, and the erosion of the breach was assumed to progress to the bottom of the dam. Brown and Rogers (1977) presented a breach model which was based on the work of Harris and Wagner.

Most recently Ponce and Tsvoglou (1981) presented a rather complex breach erosion model which coupled the Meyer-Peter and Müller sediment transport equation to the one-dimensional differential equations of unsteady flow and sediment conservation. Reservoir storage depletion was included in the upstream boundary equation used in conjunction with the unsteady flow equations. The set of differential equations was solved with a four-point implicit finite difference scheme. Flow resistance was represented through use of the Manning  $n$ . Breach width was empirically related to the rate of breach flow. A small rivulet was assumed to be initially present along the flow path. "Outflow at start of the computation is a function of the assumed initial size of the rivulet. Progressive erosion widens and deepens the rivulet, increasing outflow and erosion rate in a self-generating manner. The upper cross-section on the sloping downstream face creeps upstream across the dam top until it reaches the upstream face, whereby rate of flow and erosion increase at a faster rate. If outflow increases enough to lower the reservoir level faster than the channel bed erodes, both outflow and erosion gradually diminish. Of course, outflow will eventually decrease even if the breach bed erodes all the way down to the stream bed. This mode of failure creates the outflow hydrograph in the shape of a sharp but nevertheless gradual flood wave." Ponce and Tsvoglou compared the model's predictions with observations of a breached landslide-formed dam on the Mantaro River in Peru. The results were considered good. However, they were influenced by the judicious selection of the Manning  $n$ , the breach width-flow relation parameter, and a coefficient in the sediment transport equation, although Ponce and Tsvoglou stated that the selected values were within each one's reasonable range of variation. Also, problems of a numerical computational nature were alluded to in connection with solving the implicit finite difference unsteady flow equations. They also implied that further work was needed to improve the breach width-flow relation and

in developing a relation between the Manning  $n$  and the hydraulic/sediment characteristics of the breach channel.

The breach erosion model presented in this paper differs substantially from those previously reported. A summation of the important differences will be given after the model has been completely described in the next section.

#### MODEL DESCRIPTION

##### General

The breach erosion model (BREACH) simulates the failure of an earthen dam as shown in Fig. 2. The dam may be homogeneous or it may consist of two materials, an outer zone with distinct material properties ( $\phi$  - friction angle,  $C$  - cohesion,  $D_{50}$  - average grain size, and  $\gamma$  - unit weight) and an inner core with its  $\phi$ ,  $C$ ,  $D_{50}$ , and  $\gamma$  values. The downstream face of the dam is described by specifying the top of the dam ( $H_t$ ), the bottom elevation of the dam ( $H_b$ ) or original streambed elevation, and its slope as given by the ratio 1 (vertical) : ZD (horizontal). Then, the upstream face of the dam is described by specifying its slope as the ratio 1 (vertical) : ZU (horizontal). If the dam is man-made it is further described by specifying a flat crest width ( $W_{CR}$ ) and a spillway rating table of spillway flow vs. water elevation, in which the first elevation represents the spillway crest. Naturally formed landslide dams are assumed to not have a flat crest or, of course, a spillway.

The storage characteristics of the reservoir are described by specifying a table of surface area ( $S_s$ ) in units of acre-ft vs. water elevation, the initial water surface elevation ( $H_1$ ) at the beginning of the simulation, and a table of reservoir inflows ( $Q_i$ ) in cfs vs. the hour of their occurrence ( $T_i$ ).

If an overtopping failure is simulated, the water level ( $H$ ) in the reservoir must exceed the top of the dam before any erosion occurs. The first stages of the erosion are only along the downstream face of the dam as denoted by the line A-A in Fig. 2 where, initially, a small rectangular-shaped rivelet is assumed to exist along the face. An erosion channel of depth-dependent width is gradually cut into the downstream face of the dam. The flow into the channel is determined by the broad-crested weir relationship:

$$Q_b = 3 B_o (H - H_c)^{1.5} \quad (1)$$

in which  $Q_b$  is the flow into the breach channel,  $B_o$  is the instantaneous width of the initially rectangular-shaped channel, and  $H_c$  is the elevation of the breach bottom. As the breach erodes into the downstream face of the dam, the breach bottom elevation ( $H_c$ ) remains at the top of the dam ( $H_t$ ),

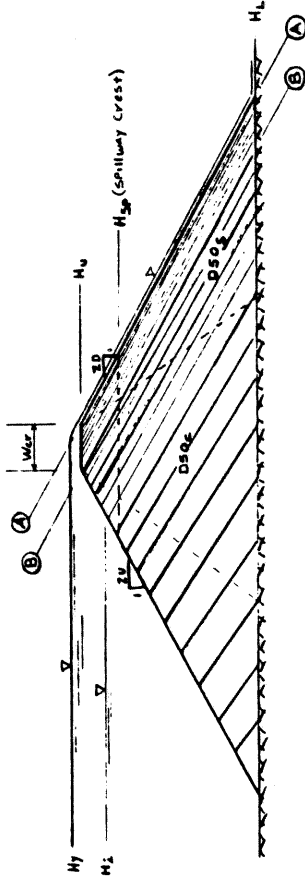


Figure 2 - Side View of Dam Showing Conceptualized Overtopping Failure Sequence.

and the most upstream point of the breach channel moves across the crest of the dam towards the dam's upstream face. When the bottom of the erosion channel has attained the position of line B-B in Fig. 2, the breach bottom ( $H_c$ ) starts to erode vertically downward. The breach bottom is allowed to progress downward until it reaches the bottom elevation of the dam ( $H_d$ ) or in unusual circumstances to an elevation ( $H_m$ ) that may be specified as lower than the bottom of the dam.

If a piping breach is simulated, the water level ( $H$ ) in the reservoir must be greater than the assumed center-line elevation ( $H_p$ ) of the initially rectangular-shaped piping channel before the size of the pipe starts to increase via erosion. The bottom of the pipe is eroded vertically downward while its top erodes at the same rate vertically upwards. The flow into the pipe is controlled by orifice flow, i.e.,

$$Q_b = 0.98(2g)^{0.5} A (H - H_p)^{0.5} \quad (2)$$

in which  $Q_b$  is the flow into the pipe,  $g$  is the gravity acceleration constant,  $A$  is the cross-sectional area of the pipe channel, and  $H - H_p$  is the hydrostatic head on the pipe. As the top elevation ( $H_{pu}$ ) of the pipe erodes vertically upward, a point is reached when the flow changes from orifice-control to weir-control. The transition is assumed to occur when the following inequality is satisfied:

$$H < H_{pu} + 2(H_{pu} - H_p) \quad (3)$$

The weir flow is then governed by Eq. (1) in which  $H_c$  is equivalent to the bottom elevation of the pipe and  $B_p$  is the width of the pipe at the instant of transition. Upon reaching the instant of flow transition from orifice to weir, the remaining material above the top of the pipe and below the top of the dam is assumed to collapse and is transported along the breach channel at the current rate of sediment transport before further erosion occurs. The erosion then proceeds to cut a channel parallel to and along the remaining portion of the downstream face of the dam between the elevation of the bottom of the pipe and the bottom of the dam. The remaining erosion process is quite similar to that described for the overtopping type of failure with the breach channel now in a position similar to line A-A in Fig. 2.

The preceding general description of the erosion process was for a man-made dam. If a landslide dam is simulated the process is identical except, due to the assumption that the landslide dam has no crest width ( $W_{cr}$ ), the erosion initially commences with the breach channel in the position of line B-B in Fig. 2. A failure mode of overtopping or piping may be initiated for a landslide-formed dam.

## Breach Width

The method of determining the width of the breach channel is a critical component of any breach model. In this model the width of the breach is dynamically controlled by two mechanisms. The first, assumes the breach has an initial rectangular shape as shown in Fig. 3. The width of the breach ( $B_0$ ) is governed by the following relation

$$B_0 = B_r y \quad (4)$$

in which  $B_r$  is a factor based on optimum channel hydraulic efficiency and  $y$  is the depth of flow in the breach channel. The parameter  $B_r$  may vary from 2.0 to 2.5 for overtopping failures with the latter recommended on the basis of current testing of the model. For piping failures,  $B_r$  is set to 1.0. The model assumes that  $y$  is the critical depth at the entrance to the breach channel, i.e.,

$$y = 2/3(H-H_c). \quad (5)$$

The second mechanism controlling the breach width is derived from the stability of soil slopes (Spangler, 1951). The initial rectangular-shaped channel changes to a trapezoidal channel when the sides of the breach channel collapse, forming an angle ( $\alpha$ ) with the vertical. The collapse occurs when the depth of the breach cut ( $H'$ ) reaches the critical depth ( $H'_k$ ) which is a function of the dam's material properties of internal friction ( $\phi$ ), cohesion ( $C$ ), and unit weight ( $\gamma$ ), i.e.,

$$H'_k = \frac{4 C \cos \phi \sin \theta'_{k-1}}{\gamma [1 - \cos (\theta'_{k-1} - \phi)]} \quad k = 1, 2, 3 \quad (6)$$

in which the subscript  $k$  denotes one of three successive collapse conditions as shown in Fig. 3, and  $\theta$  is the angle that the side of the breach channel makes with the horizontal as shown in Fig. 4. Thus, the angle ( $\theta$ ) or ( $\alpha$ ) at any time during the breach formation is given as follows:

$$\theta = \theta'_{k-1} \quad H_k < H'_k \quad (7)$$

$$\theta = \theta'_k \quad H_k > H'_k \quad (8)$$

$$B_0 = B_r y \quad k = 1 \quad (9)$$

$$B_0 = B_{om} \quad k > 1 \quad (10)$$

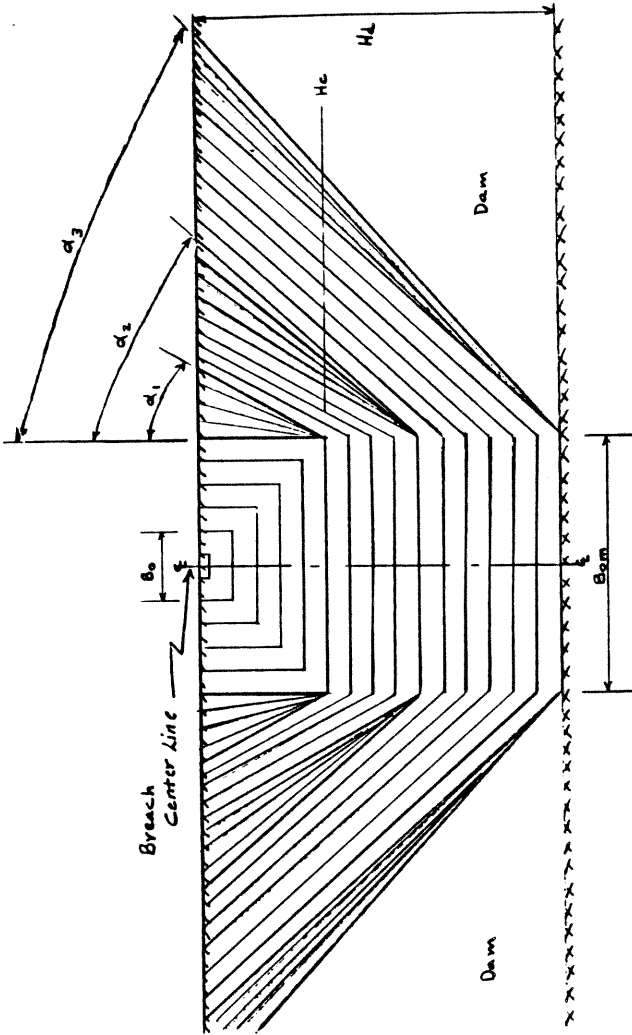


Figure 3 - Front View of Dam with Breach Formation Sequence.

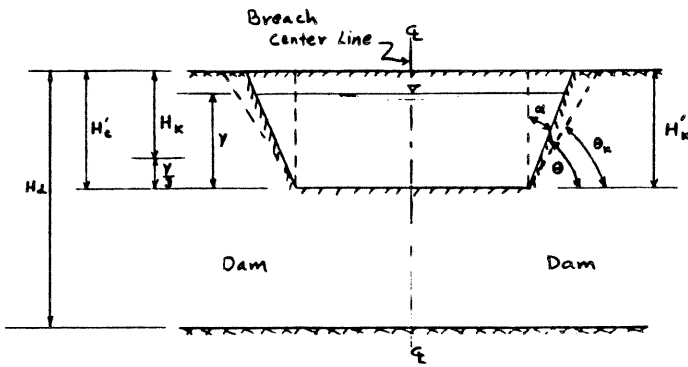


Figure 4 - Front View of Dam with Breach.

$$B_{Om} = B_r y \quad \text{when } H_1 = H'_1 \quad (11)$$

$$\alpha = 0.5\pi - \theta \quad (12)$$

where:

$$\theta'_0 = 0.5\pi \quad (13)$$

$$\theta'_k = (\theta'_{k-1} + \phi)/2 \quad k = 1, 2, 3 \quad (14)$$

$$H'_k = H'_c - y/3 \quad (15)$$

The subscript (k) is incremented by 1 at the instant when  $H_k > H'_k$ . In Eq. (15), the term (y/3) is subtracted from  $H'$  to give the actual free-standing depth of breach cut in which the supporting influence of the water on the stability of the sides of the breach is taken into account. Through this mechanism, it is possible for the breach to widen after the peak outflow through the breach has occurred since the flow depth (y) diminishes during the receding flow.

When the sides of the breach channel collapse, the breach bottom does not immediately continue to erode downward until the volume of collapsed material along the breach is removed at the rate of the sediment transport capacity of the breach channel at the instant of collapse. After this characteristically short pause, the breach bottom continues to erode downward.

When landslide dams are simulated, the relatively long breach channel lengths compared to those of man-made dams suggest that the width for the channel be computed apart from the entrance width of the breach. In this case, y in Eq. (4), (9), (11), and (15) is computed as the normal uniform depth ( $y_n$ ) in the breach channel rather than the critical depth given by Eq. (5). Equations for computing the normal channel depth are presented in a subsequent section.

#### Reservoir Level Determination

Conservation of mass is used to compute the change in the reservoir water surface elevation (H) due to the influence of reservoir inflow ( $Q_i$ ), spillway outflow ( $Q_{sp}$ ), crest overflow ( $Q_o$ ), breach outflow ( $Q_b$ ), and the reservoir storage characteristics. The conservation of mass over a time step ( $\Delta t$ ) in hours is represented by the following:

$$\bar{Q}_i - (\bar{Q}_b + \bar{Q}_{sp} + \bar{Q}_o) = S_a \frac{\Delta H}{\Delta t} \frac{43560}{3600} \quad (16)$$

in which  $\Delta H$  is the change in water surface elevation during the time interval ( $\Delta t$ ), and  $S_a$  is the surface area in acres at elevation  $H$ . All flows are expressed in units of cfs and the bar (-) indicates the flow is averaged over the time step. Rearranging Eq. (16) yields the following expression for the change in the reservoir water surface:

$$\Delta H = \frac{0.0826 \Delta t}{S_a} (\bar{Q}_i - \bar{Q}_b - \bar{Q}_{sp} - \bar{Q}_o) \quad (17)$$

The reservoir elevation ( $H$ ) at time ( $t$ ) can easily be obtained from the relation,

$$H = H' + \Delta H \quad (18)$$

in which  $H'$  is the reservoir elevation at time  $t - \Delta t$ .

The reservoir inflow ( $\bar{Q}_i$ ) is determined from the specified table of inflows ( $Q_i$ ) vs. time ( $T_i$ ). The spillway flow ( $\bar{Q}_s$ ) is determined from the specified table of spillway flows ( $Q_s$ ) vs. reservoir elevation ( $H$ ). The breach flow ( $Q_b$ ) is computed from Eq. (2) for piping flow. When the breach flow is weir-type, Eq. (1) is used when  $H_c = H_u$ ; however, when  $H_c < H_u$ , the following broad-crested weir equation is used:

$$Q_b = 3 B_o (H - H_c)^{1.5} + 2 \tan(\alpha) (H - H_c)^{2.5} \quad (19)$$

in which  $B_o$  is given by Eq. (9) or Eq. (10) and  $\alpha$  is given by Eq. (12). The crest overflow is computed as broad-crested weir flow from Eq. (1), where  $B_o$  is replaced by the crest length of the dam and  $H_c$  is replaced by  $H_u$ .

#### Breach Channel Hydraulics

The breach flow is assumed to be adequately described by quasi-steady uniform flow as determined by applying the Manning open channel flow equation at each  $\Delta t$  time step, i.e.,

$$Q_b = \frac{1.49 S^{0.5} A^{1.67}}{n P^{0.67}} \quad (20)$$

in which  $S = 1/ZD$ ,  $A$  is the channel cross-section area,  $P$  is the wetted perimeter of the channel, and  $n$  is the Manning coefficient. In this model,  $n$  is computed using the Strickler relation which is based on the average grain size of the material forming the breach channel, i.e.,

$$n = 0.034 \left( \frac{D_{50}}{305} \right)^{0.167} \quad (21)$$

in which  $D_{50}$  represents the average grain size diameter expressed in mm.

The use of quasi-steady uniform flow is considered appropriate because the extremely short reach of breach channel, very steep channel slopes ( $1/ZD$ ) for man-made dams, and even in the case of landslide dams where the channel length is greater and the slope is smaller, contribute to produce extremely small variation in flow with distance along the breach channel. The use of quasi-steady uniform flow as opposed to the unsteady flow equations as used by Ponce and Tsvoglou (1981) greatly simplifies the hydraulics and computational algorithm. Such simplification is considered commensurate with the other simplifications inherent in the treatment of the breach development in dams for which precise measurements of material properties are lacking or impossible to obtain and the wide variance which exists in such properties in many dams. The simplified hydraulics eliminates troublesome numerical computation problems and enables the breach model to require only minimal computational resources.

When the breach channel is rectangular, the following relations exist between depth of flow ( $y_n$ ) and discharge ( $Q_b$ ):

$$y_n = \frac{Q_b n^{0.6}}{1.49 B_o S^{0.5}} \quad (22)$$

in which  $B_o$  is defined by Eqs. (9-11).

When the breach channel is trapezoidal, the following algorithm based on Newton-Raphson iteration is used to compute the depth of flow ( $y_n$ ):

$$y_n^{k+1} = y_n^k - \frac{f(y_n^k)}{f'(y_n^k)} \quad (23)$$

$$f(y_n^k) = Q_b P^{0.67} - 1.49 S^{0.5} A^{1.67} \quad (24)$$

$$\text{in which} \quad A = 0.5(B_o + B) y_n^k \quad (25)$$

$$B = B_{om} + y_n \tan(\alpha) \quad (26)$$

$$P = B_{om} + y_n / \cos(\alpha) \quad (27)$$

$$f'(y_n^k) = 0.67 Q_b \frac{P'}{p^{1/3}} - 1.67 \frac{1.49}{n} S^{0.5} \bar{B} A^{0.67} \quad (28)$$

in which 
$$P' = 1/\cos(\alpha). \quad (29)$$

The superscript (k) is an iteration counter; the iteration continues until

$$|y_n^{k+1} - y_n^k| < \epsilon \quad \epsilon < 0.01 \quad (30)$$

The first estimate for  $y_n$  is obtained from the following:

$$y_n^1 = \left( \frac{Q_b n}{1.49 \bar{B} S^{0.5}} \right)^{0.6} \quad (31)$$

where:

$$\bar{B} = 0.5(B_{om} + B') \quad (32)$$

in which  $B'$  is the breach channel top width at the water depth ( $y_n$ ) at ( $t-\Delta t$ ).

#### Sediment Transport

The rate at which the breach is eroded depends on the capacity of the flowing water to transport the eroded material. For man-made dams the Meyer-Peter and Müller sediment transport relation (Morris and Wiggert, 1972) is used, i.e.,

$$Q_g = aP(SR - \tau_c)^{1.5} \quad (33)$$

where:

$Q_g$  = sediment transport rate in cfs;

$a = 27.5$ ;

$P$  = wetted perimeter of the breach channel as given by Eq. 27 for the trapezoidal shaped channel or by  $(B_o + 2y_n)$  for the rectangular breach.

$R$  = hydraulic radius ( $A/P$ );

$S$  = slope of the breach channel,  $(1/ZD)$  for

weir channels and  $[n^2 Q_b^2 / (2.21A R^{1.33})]$  for  
piping channels;

$\tau_c$  = critical shear stress = 0.0003  $D_{50} C_v$ ; and

$C_v$  = empirical factor to account for additional resistance to  
sediment transport due to vegetative cover on the  
downstream face of the dam.

For landslide dams, the duBoys relation (Morris and Wiggert, 1972) is used,  
i.e.,

$$Q_s = \frac{b}{D_{50}^{0.75}} \text{PSR}(\text{SR} - \tau_c) \quad (34)$$

where:

$$b = 671.$$

The coefficients a and b in Eqs. (33) and (34) are set at the fixed  
values, 27.5 and 671, respectively. These values were used in all test  
applications of the breach erosion model (BREACH) presented herein. It was  
considered inappropriate to vary these coefficients.

#### Breach Enlargement By Sudden Collapse

It is possible for the breach to be enlarged by a rather sudden  
collapse failure of the upper portions of dam in the vicinity of the breach  
development. Such a collapse would consist of a wedge-shaped portion of the  
dam having a vertical dimension ( $Y_c$ ) as shown in Fig. 5. The collapse would  
be due to the pressure of the water on the upstream face of the dam  
exceeding the resistive forces due to shear and cohesion which keep the  
wedge in place. When this occurs the wedge is pushed to the right in Fig. 6  
and is then transported by the escaping water through the now enlarged  
breach. When collapse occurs, the erosion of the breach ceases until the  
volume of the collapsed wedge is transported through the breach channel at  
the transport rate of the water escaping through the suddenly enlarged  
breach. A check for collapse is made at each  $\Delta t$  time step during the  
simulation. The collapse check consists of assuming an initial value for  $Y_c$   
of 10 and then summing the forces acting on the wedge of height,  $Y_c$ . The  
forces are those due to the water pressure ( $F_w$ ) and the resisting forces  
which are the shear force ( $F_{sb}$ ) acting along the bottom of the wedge, the  
shear force ( $F_{ss}$ ) acting along both sides of the wedge, the force ( $F_{cb}$ ) due  
to cohesion along the wedge bottom and ( $F_{cs}$ ), the force due to cohesion  
acting along the sides of the wedge. Thus, collapse occurs if

$$F_w > F_{sb} + F_{ss} + F_{cb} + F_{cs} \quad (35)$$

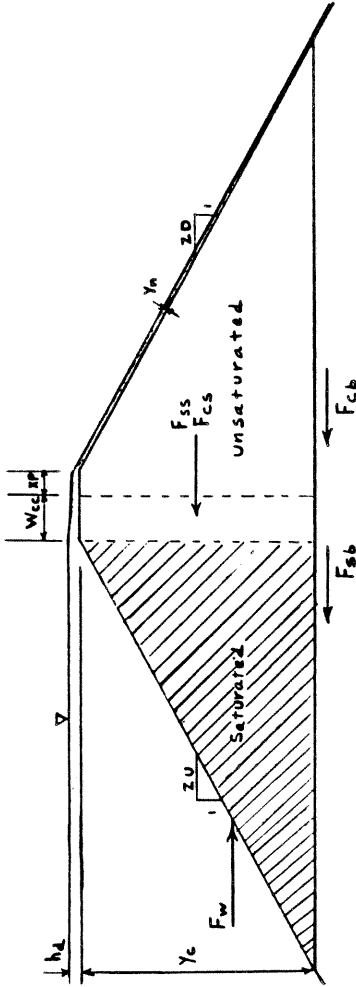


Figure 5 - Side View of Dam Showing the Forces Which Determine the Possible Collapse of the Upper Portion ( $y_c$ ) of the Dam.

where:

$$F_w = 0.5 \cdot 62.4 \bar{B} (Y_c + 2 h_d) \quad (36)$$

$$F_{sb} = \tan \phi \left[ (\gamma - 62.4) 0.5 ZU \bar{B} Y_c^2 + \gamma B W_{cc} Y_c + \right. \\ \left. \gamma 0.5 ZD \bar{B} Y_c^2 + 0.67 \cdot 62.4 h_d W_{cc} B + 62.4 ZD' B y_n Y_c \right] \quad (37)$$

$$F_{ss} = \gamma K \tan \phi Y_c^2 [W_{cc} + (ZU + ZD) Y_c] \quad (38)$$

$$F_{cb} = CB_o [W_{cc} + (ZU + ZD) Y_c] \quad (39)$$

$$F_{cs} = 2C [W_{cc} + (ZU + ZD) Y_c (B_o + 2Y_c / \cos \alpha)] \quad (40)$$

in which

$$K = (1 - \sin \phi) / (1 + \sin \phi) \quad (41)$$

$$\bar{B} = B_o + H_c \sin \alpha \quad (42)$$

$$ZD' = (1 + ZD^2)^{0.5} \quad (43)$$

and  $Y_c$ ,  $h_d$ ,  $ZU$ ,  $ZD$ ,  $W_{cc}$ ,  $y_n$  are defined in Fig. 5. The top width ( $B$ ) of the water surface in the breach channel is defined by Eq. (4) or Eq. (26), and  $\alpha$  is defined in Fig. 4 and Eq. (12).

If the inequality of Eq. (35) is not satisfied with the first trial  $Y_c$ , then no collapse occurs at this time. If it is satisfied,  $Y_c$  is increased by 2 ft and Eq. (35) is again evaluated. This cycle continues until the inequality is not satisfied. Then the final value for  $Y_c$  is assumed to be  $Y_c - 1$ .

#### Computational Algorithm

The sequence of computations in the model are iterative since the flow into the breach is dependent on the bottom elevation of the breach and its width while the breach properties are dependent on the sediment transport capacity of the breach flow, and the transport capacity is dependent on the breach size and flow. A simple iterative algorithm is used to account for the mutual dependence of the flow, erosion, and breach properties. An estimated incremental erosion depth ( $\Delta H_c$ ) is used at each time step to start the iterative computation. This estimated value can be extrapolated from previously computed incremental erosion depths after the first few time steps. The computational algorithm follows:

1. increment the time:  $t = t' + \Delta t$ ;
2. compute  $H_c$  using estimated  $\Delta H_c'$ :  $H_c = H_c' - \Delta H_c'$ ;

3. compute reservoir elevation:  $H = H' + \Delta H'$ , where  $\Delta H'$  is an estimated incremental change in the reservoir elevation as obtained by extrapolation from previous changes and  $H'$  is the reservoir elevation at time ( $t'$ );
4. compute  $\bar{Q}_{sp}$ ,  $\bar{Q}_1$ ,  $\bar{Q}_o$  associated with elevation  $H$ ;
5. compute  $\Delta H$  from Eq. (17) using the previously computed breach flow ( $Q_b$ );
6. compute reservoir elevation:  $H = H' + \Delta H$ ;
7. compute breach flow ( $Q_b$ ) using Eq. (1), Eq. (2), or Eq. (19);
8. correct breach flow for downstream submergence:
 
$$Q_b = S_b Q_b$$
 where  $S_b = 1.0 - \left( \frac{y_c - H_c}{H - H_c} - 0.67 \right)^3$  in which  $y_c$  is the tailwater depth due to the total outflow ( $Q_b + Q_{sp} + Q_o$ ), and is computed from the Manning equation applied to the tailwater cross-section;
9. compute  $B_o$ ,  $\alpha$ ,  $B$ ,  $P$ , and  $R$  for the breach channel using Eqs. (9-12, 26-27);
10. compute sediment transport rate ( $Q_s$ ) from Eq. (33) or Eq. (34);
11. compute  $\Delta H_c$  as follows:  $\Delta H_c = 3600 \Delta t Q_s / [P_o L (1 - P_{or})]$ 

in which  $L$  is the length of the breach channel which may be easily computed from the geometric relations shown in Fig. 2,  $P_{or}$  is the porosity of the breach material, and  $P_o$  is the total perimeter of the breach,  $P_o = B_o + 2(H_u - H_c) / \cos \alpha$ ;
12. compute  $\Delta H_c$  with the estimated value  $\Delta H_c'$ :
 

if  $100(\Delta H_c' - \Delta H_c) / \Delta H_c' < E$ , where  $E$  is an error tolerance in percent (an input to the model having a value between 0.1 and 1.0), then the solution for  $\Delta H_c$  and the associated outflows  $Q_b$ ,  $Q_s$  and  $Q_o$  are considered acceptable; if the above inequality is not satisfied step (2) is returned to with the recently computed  $\Delta H_c$  replacing  $\Delta H_c'$ ; this cycle is repeated until convergence is attained, usually within 1 or 2 iterations.
13. check for collapse;
14. extrapolate estimates for  $\Delta H_c'$  and  $\Delta H'$ ;

15. if  $t$  is less than the specified duration of the computation ( $t_a$ ) return to step 1; and
16. plot the outflow hydrograph consisting of the total flow ( $Q_b + Q_g + Q_o$ ) computed at each time step.

#### Computational Requirements

The basic time step ( $\Delta t$ ) is specified; however when rapid erosion takes place the basic time step is automatically reduced to  $\Delta t/20$ . The specified value for the basic time step is usually about 0.05 hrs with slightly larger values acceptable for landslide dams. For typical applications, the BREACH model requires less than 10 seconds of CPU time on a Prime 750 computer and less than 2 seconds on an IBM 360/195 computer, both of which are main-frame computers. Although it has not been used on micro-computers, it would be quite amenable to such applications.

The model has displayed a lack of numerical instability or convergence problems. The computations show very little sensitivity to a reasonable variation in basic time step size. Numerical experimentation indicates that as the time step is increased by a factor of 4, the computed peak flow ( $Q_p$ ), time of peak ( $T_p$ ), and final breach dimensions vary by less than 10, 4, and 0.5 percent, respectively.

#### Comparison With Previous Models

The BREACH model differs from the models of Cristofano (1965) and Harris and Wagner (1967) in the following significant ways:

- 1) The sediment transport algorithms utilized, 2) the method used for changing the breach shape and width, 3) the delay in breach erosion downward until the downstream face has been sufficiently eroded, 4) the introduction of a possible collapse mechanism for breach enlargement, 5) the accommodation of a piping failure mode, and 6) the consideration of possible tailwater submergence effects on the breach flow. Similarities are their simplicity of the computational algorithm, the use of the  $D_{50}$  grain size and internal friction angle ( $\phi$ ), and the assumption of quasi-steady uniform flow hydraulics.

The BREACH model differs from the model reported by Ponce and Tsivoglou (1981) in the following significant ways: 1) items 1,2,4,5, and 6 as stated above, 2) the much simpler computational algorithm used in BREACH, 3) the use of the internal friction angle, 4) the use of the Strickler equation for determining the Manning  $n$  and 5) consideration of spillway flows for man-made dams. Similarities between the two models include the use of the Meyer-Peter and Müller transport relation, the gradual development of the breach channel along the downstream face of the dam prior to its erosion vertically through the dam's crest, the use of the Manning  $n$  for the breach channel hydraulics, and the way in which the reservoir hydraulics are included in the development of the breach.

## MODEL APPLICATIONS

The BREACH model was applied to three earthen dams to determine the outflow hydrograph produced by a gradual breach of each. The first was an actual piping failure of the man-made Teton dam in Idaho, the second was an actual overtopping failure of the landslide-formed dam which blocked the Mantaro River in Peru, and the third was a hypothetical piping failure of the landslide dam which blocks the natural outlet of Spirit Lake near Mount St. Helens in Washington.

## Teton Dam

The Teton Dam, a 300 ft high earthen dam with a 3000 ft long crest and 262 ft depth of stored water amounting to about 250,000 acre-ft, failed on June 5, 1976. According to a report by Ray, et. al (1976) the failure started as a piping failure about 10:00 AM and slowly increased the rate of outflow until about 12:00 noon when the portion of the dam above the piping hole collapsed and in the next few minutes (about 12 minutes according to Blanton (1977)) the breach became fully developed allowing an estimated 1.6 to 2.8 million cfs (best estimate of 2.3) peak flow (Brown and Rogers, 1977) to be discharged into the valley below. At the time of peak flow the breach was estimated from photographs to be trapezoidal shape having a top width at the original water surface elevation of about 500 ft and side slopes of about 1 vertical to 0.5 horizontal. After the peak outflow the outflow gradually decreased to a comparatively low flow in about 1.7 hours as the reservoir volume was depleted and the surface elevation receded. The downstream face of the dam had a slope of 1:2 and the upstream face 1:2.5. The crest width was 35 ft and the bulk of the breach material was a  $D_{50}$  size of 0.03 mm. The inflow to the reservoir during failure was insignificant and the reservoir surface area at time of failure was about 1950 acre-ft.

The BREACH model was applied to the piping generated failure of the Teton Dam. The centerline elevation for the piping breach was 180 ft above the bottom of the dam, and an initial width of 1 ft was used for the assumed square-shaped pipe. The material properties of the breach were assumed as follows:  $\phi = 40$  deg,  $C = 250$  lb/ft<sup>2</sup>, and  $\gamma = 100$  lb/ft<sup>3</sup>. The Strickler equation was judged not to be applicable for the extremely fine breach material, and the  $n$  value was computed as 0.013 from a Darcy friction factor based on the  $D_{50}$  grain size and the Moody curves (Morris and Wiggert, 1972). The computed outflow hydrograph is shown in Fig. 6. The timing, shape, and magnitude of the hydrograph compares quite well with the estimated actual values. The computed peak outflow of 2.3 million cfs agrees with the best estimate made by the U.S. Geological Survey and the time of occurrence is also the same. The computed breach width of 470 ft agrees closely with the estimated value of 500 ft at the elevation of the initial reservoir water surface. A larger estimated actual breach width of 650 ft breach width was reported by Brown and Rogers (1977); however this was the final breach width after additional enlargement of the breach occurred. The (BREACH) model produced a final width of 570 ft when the reservoir water elevation has receded to near the reservoir bottom; the

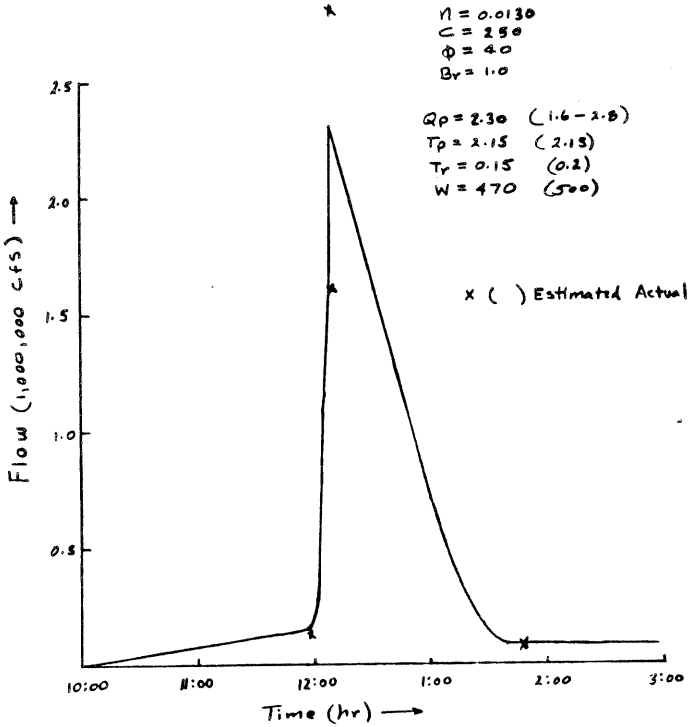


Figure 6 - Teton Dam: Predicted and Observed Breach Outflow Hydrograph and Breach Properties.

additional widening of the breach during the recession of the outflow is due to the influence of the depth ( $y$ ) in Eq. (15)

Sensitivities of the peak breach outflow ( $Q_p$ ) and the top width ( $W$ ) of the trapezoidal-shaped breach to variations in the specified breach material properties consisting of the flow resistance factor (Manning  $n$ ), cohesive strength ( $C$ ), and internal friction angle ( $\phi$ ) are shown in Fig. 7. The dashed lines apply to the Teton simulation. Peak outflow is not affected by the Manning  $n$ ; however it is sensitive to the  $C$  and  $\phi$  values which control the enlargement of the breach width. Although  $Q_p$  is sensitive to  $C$  and  $\phi$ ,  $C$  can vary by a factor of 0.2 to 4.0 times the selected value of 250 with less than 35% variation in  $Q_p$ . Likewise the  $\phi$  value may vary by  $\pm 5$  degrees with less than 20% variation in  $Q_p$ . The breach width was insensitive to the Manning  $n$ , somewhat sensitive to variations in the cohesion ( $C$ ), and almost equally sensitive to the  $\phi$  value as was the peak outflow.

Sensitivities of the time of peak outflow ( $T_p$ ) and the time of rise ( $T_r$ ) to variations in  $n$ ,  $C$ , and  $\phi$  as shown by the dashed lines in Fig. 8.  $T_p$  is sensitive to the Manning  $n$  but is not sensitive to variations in the  $C$  and  $\phi$  values. The Manning  $n$  affects the rate of breach development in the early phase of the breaching process during the initial piping formation. This is reflected in the time required for the gradual increase in outflow prior to the rather sudden and dramatic occurrence of the rising limb of the hydrograph in Fig. 6. The time of rise ( $T_r$ ) is somewhat sensitive to variations in  $n$ ,  $C$ , and  $\phi$ ; however, the apparent variation of up to 25% is not significant when expressed in actual values of less than 0.10 hrs.

#### Mantaro Landslide Dam

A massive landslide occurred in the valley of the Mantaro River in the mountainous area of central Peru on April 25, 1974. The slide, with a volume of approximately  $5.6 \times 10^{10}$  ft<sup>3</sup>, dammed the Mantaro River and formed a lake which reached a depth of about 560 ft before overtopping during the period June 6-8, 1974 (Lee and Duncan, 1975). The overtopping flow very gradually eroded a small channel along the approximately 1 mile long downstream face of the slide during the first two days of overtopping. Then a dramatic increase in the breach channel occurred during the next 6-10 hrs resulting in a final trapezoidal-shaped breach channel approximately 350 ft in depth, a top width of some 650-750 ft, and side slopes of about 1:1. The peak flow was estimated at 353,000 cfs as reported by Lee and Duncan (1975), although Ponce and Tsivoglou (1981) reported an estimated value of 484,000 cfs. The breach did not erode down to the original river bed; this caused a rather large lake to remain after the breaching had subsided some 24 hrs after the peak had occurred. The slide material was mostly a mixture of silty sand with some clay resulting in a  $D_{50}$  size of about 11 mm with some material ranging in size up to 3 ft boulders.

The BREACH model was applied to the Mantaro landslide-formed dam using the following parameters:  $ZU = 17$ ,  $ZD = 7.5$ ,  $H_u = 560$  ft,  $D_{50} = 11$  mm,  $P_c = 0.5$ ,  $S = 1200$  acres,  $C = 400$  lb/ft<sup>2</sup>,  $\phi = 35$  deg,  $\gamma = 100$  lb/ft<sup>3</sup>,  $B_c^{OR} = 2.5$ , and  $\Delta t = 0.1$  hr. The Manning  $n$  was estimated by Eq. (21) as 0.020

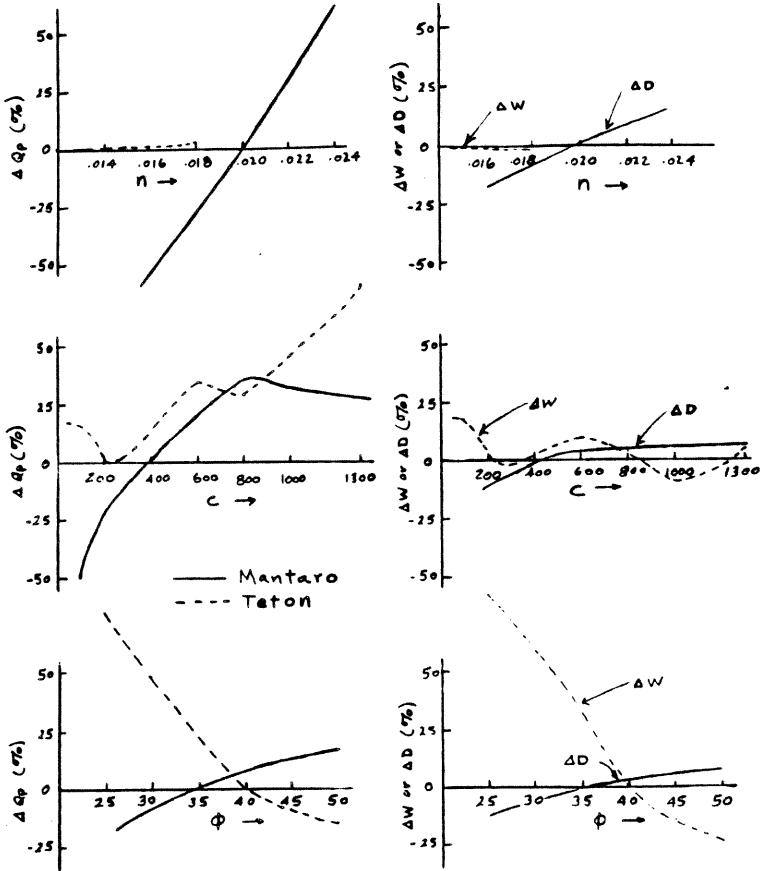


Figure 7 - Sensitivity of Mantaro and Teton Predictions of Peak Outflow ( $Q_p$ ) and Breach Width ( $W$ ) and Breach Depth ( $D$ ) to changes in the properties of the Dam: Friction Angle ( $\phi$ ), Cohesion ( $C$ ), and Manning  $n$ .

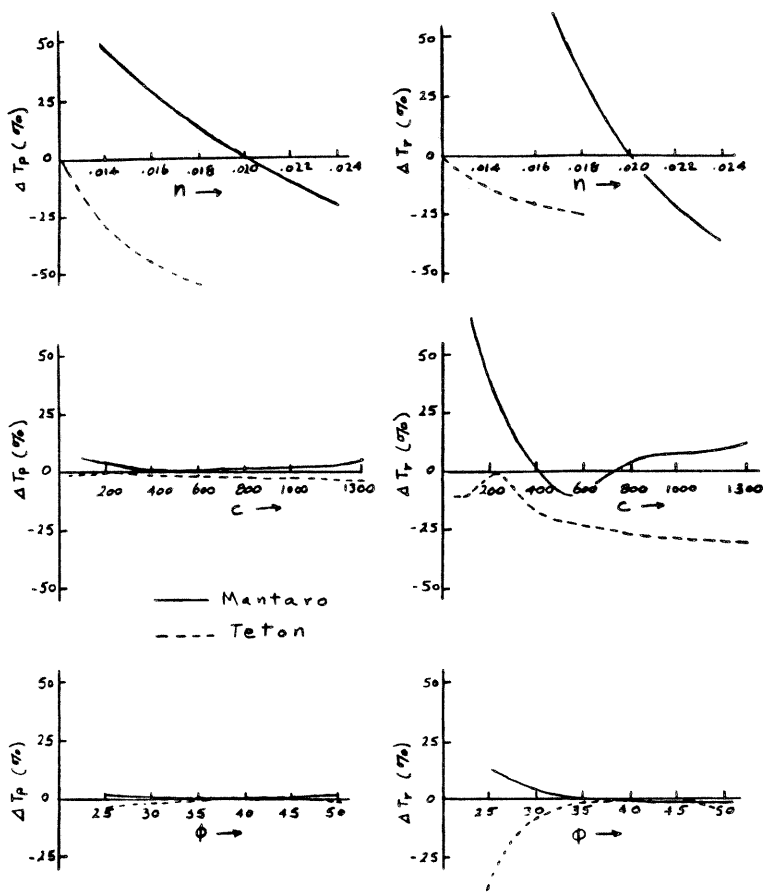


Figure 8 - Sensitivity of Mantaro and Teton Predictions of Time of Peak Outflow (Tp) and Time of Rise of Peak Outflow (Tr) to changes in the Properties of the Dam: Friction Angle ( $\phi$ ), Cohesion (C), and Manning n.

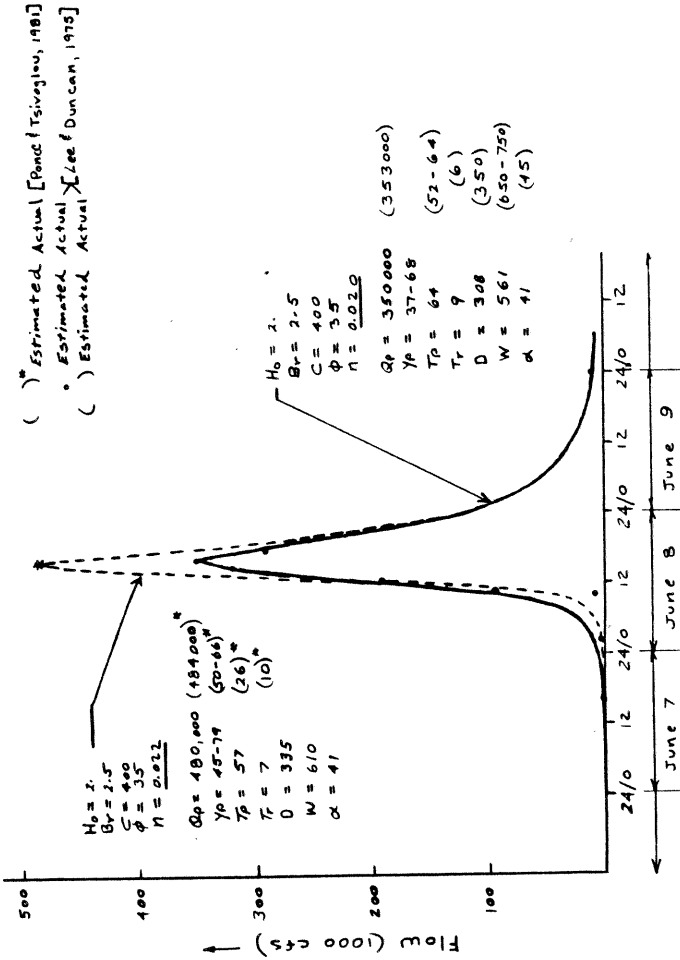


Figure 9 - Mantaro Landslide Dam: Predicted and Observed Breach Outflow Hydrograph and Breach Properties.

and the initial breach depth was assumed to be 0.5 ft. The computed breach outflow is shown by the solid line in Fig. 9 along with the estimated actual values. The timing of the peak outflow and its magnitude are very similar except for a somewhat more gradual rising limb of 10 hr compared to the estimated actual of 6 hr. The dimensions of the gorge eroded through the dam are similar as shown by the values of  $D$ ,  $W$ , and  $\alpha$  in Fig. 9. The hydrograph denoted by the dashed lines is produced if only the Manning  $n$  is increased to 0.0225, a value which for the Mantaro slide would be computed by Eq. (21) if the  $D_{50}$  size were replaced by a  $D_{60}$  size. The dashed hydrograph is very similar except it has a peak nearly the same as that reported by Ponce and Tsvoglou (1981). The breach size is somewhat larger as indicated by the  $D$ ,  $W$ , and  $\alpha$  values associated with the dashed hydrograph in Fig. 9. In particular, the depth of breach erosion is greater and nearer the estimated value of 350 ft. The influence of the Manning  $n$  on the magnitude of the peak outflow and the breach dimensions is illustrative of the more voluminous landslide dam's sensitivity to this parameter.

This is further illustrated by the solid lines (Mantaro Dam) in Fig. 7 where  $Q_p$  is seen to be very sensitive to variations in the Manning  $n$  while the depth of breach ( $D$ ) is less sensitive. The peak outflow is also sensitive to the cohesion ( $C$ ) value, although a change in  $C$  of 0.25 to 4.0 times the value used in the simulation produced variations in  $Q_p$  of less than  $\pm 35\%$ .  $D$  is not sensitive to the changes in  $C$ . Both  $Q_p$  and  $D$  are not very sensitive to the  $\phi$  value, variations in each being less than  $\pm 15\%$  for a complete range of physically relevant values of the friction angle ( $\phi$ ).

Sensitivities of  $T_p$  and  $T_r$  to variations in  $n$ ,  $C$ , and  $\phi$  are shown by the solid lines (Mantaro Dam) in Fig. 8. The time ( $T_p$ ) at which the peak outflow occurs is very sensitive to the Manning  $n$ . As in the man-made Teton Dam, it is the duration of the gradual increase in outflow prior to a rather dramatic development of the rising limb that depends on the value of the Manning  $n$ . Also, the time of rise ( $T_r$ ) is sensitive to the  $n$  value; the values of  $T_r$  varied from 6 to 16 hr as the  $n$  varied from 0.024 to 0.016. Neither  $T_p$  nor  $T_r$  is sensitive to the internal friction angle ( $\phi$ ).

#### Spirit Lake Blockage

The violent eruption of Mount St. Helens on May 18, 1980, in Washington, produced a massive debris avalanche which moved down the north side of the volcano depositing about 105 billion  $\text{ft}^3$  of materials in the upper 17 miles of the North Fork of the Toutle River valley and blocking the former outlet channel of Spirit Lake with deposits of up to 500 ft deep (Swift and Kresch, 1983). Spirit Lake, itself was drastically changed by the avalanche; the existing lake has a maximum volume of 314,000 acre-ft at the elevation of 3475 msl when breaching of the debris blockage is anticipated. To avoid this the Corps of Engineers have installed temporary pumps to maintain the lake level at about elevation 3462 (275,000 acre-ft) and are expecting to complete in the near future a permanent outlet channel which will bypass the debris dam and maintain safe lake levels.

Greater than normal precipitation, failure of the pumping system, and/or addition of more avalanche material from another eruption of the volcano could cause the lake level to exceed elevation 3475 and possibly cause the debris dam to fail. Such a hypothetical breach was simulated using the BREACH model.

An initial piping failure was assumed to occur at elevation 3448. The following parameters were determined from physical considerations:  $H_u = 3475$ ,  $H_l = 3448$ ,  $H_b = 3320$ ,  $ZD = 30$ ,  $ZU = 22$ ,  $D_{50} = 7$ ,  $n = 0.018$  from Eq. (21),  $P_P = 0.32$ ,  $\gamma = 100$ ,  $\phi = 35$ ,  $C = 150$ ,  $B_r = 1.5$ , an initial pipe of width 0.25 ft, and  $\Delta t = 0.20$  hr. The simulated outflow hydrograph shown in Fig. 10 has a peak of about 550,000 cfs occurring 15 hrs after the start of failure. The time of rise ( $T_r$ ) is about 2 hr. The final breach dimensions are:  $D = 155$  ft,  $W = 420$  ft, and  $\alpha = 50$  deg. Sensitivity tests indicate about a 20% variation in the peak flow may occur with expected variation in the internal friction angle and cohesion values. The predicted outflow hydrograph from Spirit Lake was used in a hazard investigation of possible mud flows along the Toutle and Cowlitz Rivers by Swift and Kresch (1983).

#### SUMMARY

A breach erosion model (BREACH) based on principles of hydraulics, sediment transport, and soil mechanics is described. The model uses equations of weir or orifice flow to simulate the outflow entering a channel that is gradually eroded through an earthen man-made or landslide-formed dam. Conservation of reservoir inflow, storage volume, and outflow (crest overflow, spillway flow, and breach flow) determines the time-dependent reservoir water elevation which along with the predicted breach bottom elevation determines the head controlling the reservoir outflow. A sediment transport relation, either Meyer-Peter and Müller or duBoys, is used to predict the transport capacity of the breach flow whose depth is determined by a quasi-steady uniform flow relation (the Manning equation applied at each  $\Delta t$  time step during the breach simulation). Breach enlargement is governed by the rate of erosion which is a function of the breach bottom slope and depth of flow and by the extent of collapse that occurs to the sides of the breach due to one or more sequential slope failures. The breach material properties (internal friction angle ( $\phi$ ) and cohesive strength ( $C$ )) are critical in determining the extent of enlargement of the trapezoidal-shaped breach. Another parameter, the Manning  $n$ , is most critical in determining the rate of breaching of landslide dams but is much less important in the breaching of the much smaller man-made dams. The Manning  $n$  may be predicted on the basis of the grain size of the breach material by the Strickler equation or via the Darcy friction factor-grain size- $n$  relation. The dam may consist of two different materials, an outer layer and an inner core. Piping or overtopping failure modes can be simulated as well as sudden collapses of sections of the breach due to excessive hydrostatic pressure. The model has the potential to determine if a breach will develop sufficiently during an overtopping of the dam to cause a catastrophic release of the reservoir's stored water. The BREACH model has a simple iterative computational structure which has well-behaved and

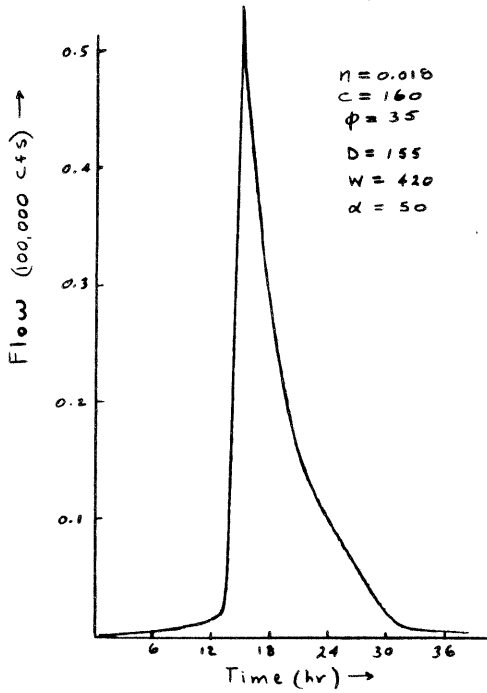


Figure 10 - Spirit Lake Landslide Dam: Predicted Breach Outflow Hydrograph.

efficient numerical properties. A few seconds of computer time is required for a typical application.

The model is tested on a man-made dam (Teton Dam) which failed by an initial piping which progressed to a weir type free surface breach. The predicted outflow hydrograph and breach size and shape compare favorably with estimated actual values. The predictions are somewhat sensitive to the values of  $\phi$  and C which were estimated from a grain size and a qualitative description of the dam's material composition.

The model is also tested on the naturally formed landslide blockage of the Mantaro River in Peru which was overtopped and developed a large gorge which resulted in the gradual release of three-fourths of its stored water. The model predictions compared well with estimated observed values. The Manning n is critical to the prediction of the rate of breaching of massive landslide dams; however if it is selected on the basis of the breach material's grain size the results are within a reasonable range of variation.

It is considered that further testing of the model to assess its ability to predict overtopping failures of man-made dams is warranted and that its basic structure is suited to the resources (data and computational) which are commonly available to hydrologists/engineers during a detailed investigation of potential dam-failure flooding.

#### REFERENCES

- Blanton, J.O. III. 1977. Flood plain inundation caused by dam failure. Proceedings of the Dam-Break Flood Routing Workshop. Water Resources Council, 47-64.
- Brown, R.J., and D.C. Rogers. 1977. A simulation of the hydraulic events during and following the Teton Dam failure. Proceedings of the Dam-Break Flood Routing Workshop. Water Resources Council, 131-163.
- Cristofano, E.A. 1965. Method of computing erosion rate for failure of earthfill dams. United States Bureau of Reclamation, Denver, Colorado.
- Fread, D.L. 1977. The development and testing of a dam-break flood forecasting model. Proceedings of the Dam-Break Flood Routing Workshop. Water Resources Council, 164-197.
- Fread, D.L. 1980. Capabilities of NWS model to forecast flash floods caused by dam failures. Proceedings of the Second Conference on Flash Floods. American Meteorological Society, 171-178.
- Fread, D.L. 1982. DAMBRK: The NWS dam-break flood forecasting model. Hydrologic Research Laboratory, National Weather Service, Silver Spring, MD., 56 p.

- Lee, K.L., and J.M. Duncan. 1975. Landslide of April 25, 1974 on the Mantaro River, Peru. National Academy of Sciences, Washington, D.C., 72 p.
- Morris, H.M., and J.M. Wiggert. 1972. Applied Hydraulics in Engineering. The Ronald Press Co., New York, 69-70, 290, 451-452, 460.
- Ponce, V.M., and A.J. Tsivoglou. 1981. Modeling of gradual dam-breaches, Journal of Hydraulics Division, American Society of Civil Engineers, 107(HY6):829-838.
- Ray, H.A., L.C. Kjelstrom, E.G. Crosthwaite, and W.H. Low. 1976. The flood in southeastern Idaho from Teton Dam failure of June 5, 1976. Open File Report, U.S. Geological Survey, Boise, Idaho.
- Spangler, M.G. 1951. Soil Engineering. International Textbook Co., Scranton, PA., 321-323.
- Swift, C.H. III and D.L. Kresch. 1983. Mudflow hazards along the Toutle and Cowlitz Rivers from a hypothetical failure of Spirit Lake blockage. Water-Resources Investigations Report 82-4125, U.S. Geological Survey, Tacoma, Washington, 10 p.